Nanoscale Thermal Management of Single SnO_2 Nanowire: pico-Joule Energy Consumed Molecule Sensor

Gang Meng,[†] Fuwei Zhuge,[†] Kazuki Nagashima,[†] Atsuo Nakao,[‡] Masaki Kanai,[†] Yong He,[†] Mickael Boudot,[†] Tsunaki Takahashi,[§] Ken Uchida[§] and Takeshi Yanagida*[,†]

[†] Institute for Materials Chemistry and Engineering, Kyushu University, 6-1 Kasuga-Koen, Kasuga, Fukuoka 816-8580, Japan

[‡] Panasonic Corporation, 1006 Kadoma, Kadoma City, Osaka 571-8506, Japan

[§] Department of Electrical Engineering, Keio University, 3-14-1 Hiyoshi Kouhokuku Yokohama 223-8522, Japan

Outline

Part I Nanowire properties and procedures to fabricate suspended device

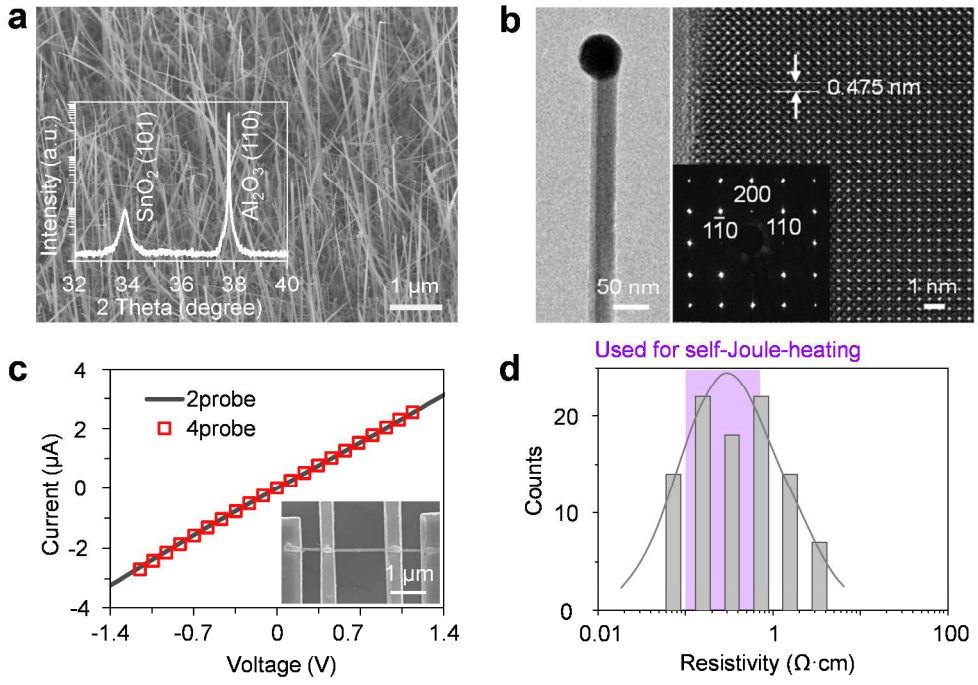

Figure S1. Structural and electrical properties of SnO_2 nanowires. (a) SEM image and XRD data of SnO_2 nanowires grown on Al_2O_3(110) substrate. (b) TEM, HRTEM and SAED data, demonstrating a single-crystallite structure of nanowire. (c) Typical 2-probe and 4-probe current-voltage (I-V) data of Ti/Au contacted nanowire devices. The device image is shown in the inset. (d) The resistivity distribution data.

SnO_2 nanowires were grown on on Al_2O_3(110) substrate by Au catalyzed vapor-liquid-solid (VLS) method.[1,2] Fig.S1 (a) shows the SEM image and XRD data of SnO_2 nanowires. Fig. S1(b) presents the TEM characterizations. Fig. S1(c) gives the typical 2-probe and 4-probe current-voltage (I-V) results of SnO_2 nanowires with Ti/Au electrodes, revealing the relatively low contact resistance ($R_{contact}/R_{4\text{-probe}} < 2\%$), which is an

important prerequisite for an efficient self-Joule-heating.[3] SnO_2 nanowires with resistivity range of 0.4 ± 0.3 Ω·cm were prescreened for the following self-Joule-heating experiments, shown in Fig.S1(d).

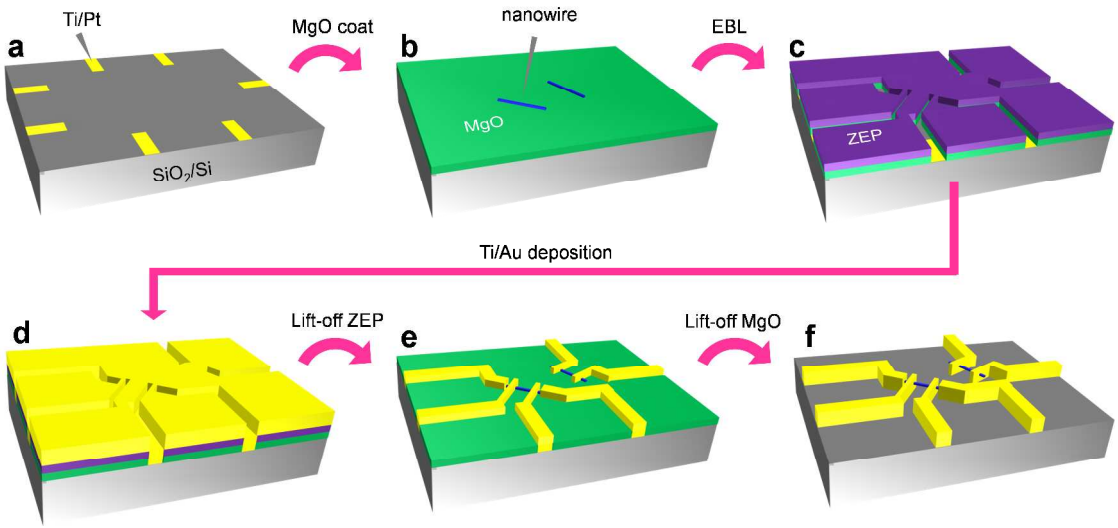

Figure S2. Schematic procedure to fabricate suspended SnO_2 nanowire devices. (a) SiO_2/Si (or PEN) substrate with predefined Ti/Pt electrodes. (b) Depositing MgO sacrificial layer (100 nm) and dispersing SnO_2 nanowires. (c) Spin coating of ZEP resist, EBL drawing, development and etching uncovered MgO layer. (d) Depositing Ti/Au (1nm/300nm) electrode. (e) Lift-off ZEP resist. (f) Dissolving MgO sacrificial layer by dilute HCl solution.

Part II Analysis of self-Joule-heating in nanowire device

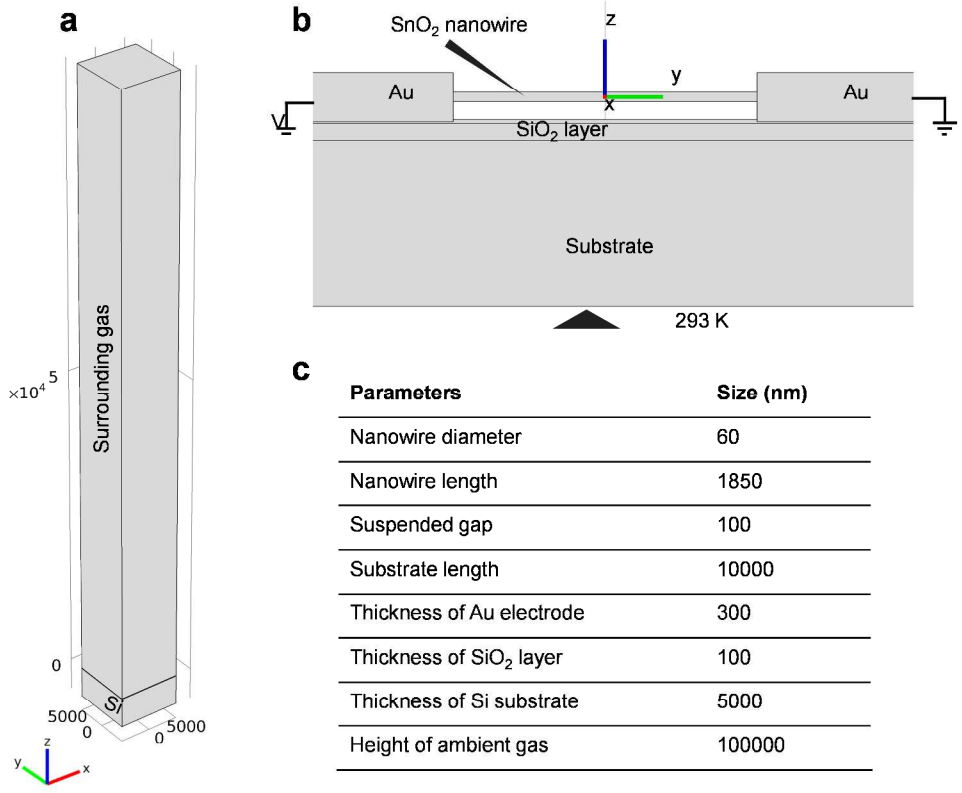

Parameters	Size (nm)
Nanowire diameter	60
Nanowire length	1850
Suspended gap	100
Substrate length	10000
Thickness of Au electrode	300
Thickness of SiO_2 layer	100
Thickness of Si substrate	5000
Height of ambient gas	100000

Figure S3. Detailed information of the simulation model. (a) Geometrical image of employed simulation model. (b) Cross-sectional view of the device area. Domain information, electrical boundary condition (voltage bias *V* and ground electrode) and temperature boundary condition (the temperature of device backside is set to be the ambient temperature of 293 K) are marked. (c) Typical dimensions of domains.

Evaluating and programing the temperature of self-heated nanowire are important issues for the practical sensor operation, as investigations of micro-hotplates have done in the past two decades.[4-7] Because of fundamental difficulties to probe the temperature at nanoscale,[8] a comprehensive study of device configurations (dimension, physical

parameters of nanowire) dependent self-Joule-heating has been difficult. In this work, we have performed COMSOL simulations, a model is shown in Figure S3. Applying a voltage bias on the nanowire device would generate the Joule heat. By considering the low power of heat source (< 100 μW), the temperature increase of substrate is negligible. Therefore, we assign the temperature of device backside to be 293 K. Based on fundamental knowledge of heat transfer, three heat transfer modes (conduction, convection and radiation) may occur in a heated nanowire. The net heat power (ΔP) determines the temperature (T) at equilibrium.

$$\Delta P = P_{Joule} - P_{solid-cond} - P_{gas-cond} - P_{conv} - P_{rad} \quad \text{(Eq-S1)}$$

where, P_{Joule}, $P_{\text{solid-cond}}$, $P_{\text{gas-cond}}$, P_{conv} and P_{rad} represent the power of Joule heat source, the power of conduction from nanowire to solid electrodes and/or substrate, the power of conduction from nanowire to gas surrounding, the power of convection and the power of radiation, respectively.

$$\Delta P \cdot t = c \cdot m \cdot (T - T_{amb}) \quad \text{(Eq-S2)}$$

where, t is a time, c is the specific heat capacity of SnO_2 (c= 52.6 J/mol·K),[9] m is the mass of SnO_2 nanowire and T_{amb} is the ambient temperature.

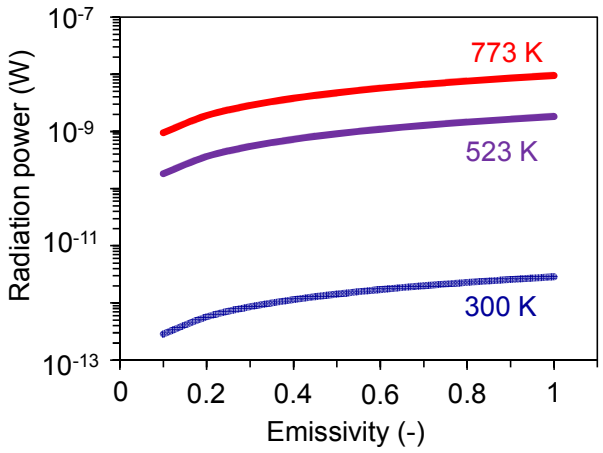

Figure S4. Radiation power from a self-heated SnO_2 nanowire as a function of emissivity and nanowire temperature. Radiation power is less than 10^{-8} W for a nanowire heated to 773 K, even overestimating the nanowire as black-body (ε=1).

Among all the possible dissipation routes listed in Eq. S1, the convection process is negligible in our experimental configurations due to the absence of gas flow in our experiments. Radiation can be estimated by the Stefan-Boltzmann law:[10]

$$P_{rad} = \varepsilon\sigma A(T^4 - T_{amb}{}^4) \qquad \text{(Eq-S3)}$$

where, ε is emissivity (ε<1), σ is Stefan-Boltzmann constant (σ=5.67×10^{-8} W/m^{2}K^4),[11] A is the surface area of heat source. We estimated the radiation power by assuming a homogeneous temperature field. The radiation power is negligible (<10^{-8} W for T=773 K), even overestimating nanowire as a black-body (ε=1), as shown in Figure S4. Therefore, the heat conduction (nanowire to electrode/substrate and nanowire to gas surrounding) should be crucial for heat dissipation of self-heated nanowires.

Fourier conduction law is given as

$$\frac{\Delta Q}{\Delta t} = -\kappa A \frac{\Delta T}{\Delta x} \qquad \text{(Eq-S4)}$$

The heat flow rate ($\Delta Q/\Delta t$) is proportional to the thermal conductivity (κ), the interface area (*(A)* and the temperature gradient ($\Delta T/\Delta x$). As can be seen, thermal conductivity of nanowire (κ_{SnO2}) plays a crucial role on the equilibrium temperature. Thus, the determination of κ is important for a semi-quantitative analysis of self-Joule-heating. Unfortunately, the bulk conductivity (55 W/mK)[12] is inappropriate for simulation due to increased phonon-boundary scattering in quasi-one-dimensional nanowire.[13] In this work, we measured κ of SnO_2 nanowire by 3-omega method,[14] The generated $V_{3\omega}$ as a function of cubic 1ω current ($I_{1\omega}$) was plotted in Figure 1f. Thermal conductivity of as-synthesized SnO_2 nanowires at room temperature (RT) can be estimated by fitting Figure 1f, based on the following equation:[14]

$$V_{3\omega} = \frac{4RR'l}{\pi^4 \kappa S} I_{1\omega}^{\ 3} \qquad \text{(Eq-S5)}$$

where, R is 4-probe resistance of nanowire at RT, R' is temperature coefficient of resistance at RT, deduced by linear fitting of Figure S5 (from 293 to 393 K). l is the length of nanowire between two inner electrodes, S is the cross section area of nanowire. Thermal conductivity of present SnO_2 nanowire (diameter of 79 nm) is ~2 W/mK, which is much lower than their bulk counterparts (55 W/mK)[12] and thus offers great benefits for an efficient self-Joule-heating, as seen in Figure 1e. It should be noted that we utilized a

fixed κ (2 W/mK) for the simulations for the sake of simplicity. This can lead to an underestimation of the simulated temperature in the case of (1) high input Joule power (κ is reduced at high temperature [12]) and (2) thinner nanowires (κ is reduced [15]).

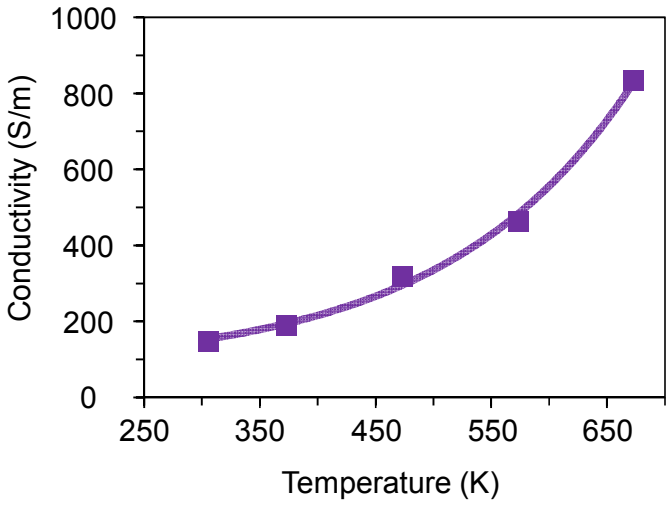

Figure S5. Temperature dependence of the electrical conductivity of SnO_2 nanowires. Experimental points (violet squares) and the fitting curve used for calculating thermal conductivity and temperature mapping of nanowires.

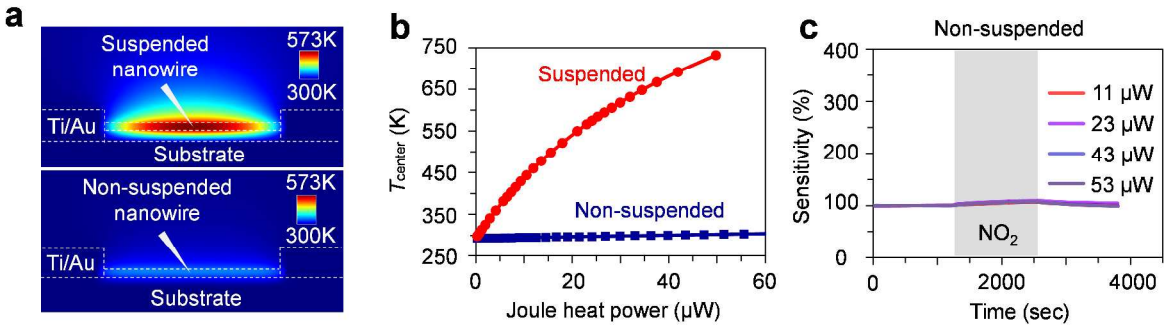

Figure S6. Importance of suspended configuration for an efficient self-Joule-heating. (a) Joule heat power dependent temperature for both suspended and non-suspended nanowire devices. (The dimension and physical parameters of nanowires are same). (b) Temperature field mapping of a suspended nanowire (P=25 μW) and non-suspended (P=50 μW), inferring noticeable heat conduction into the underlying substrate for non-suspended device. (c) NO_2 response of non-suspended SnO_2 device. We failed to observe the enhancement of sensitivity by increasing Joule power up to 53 μW, implying a low temperature of non-suspended nanowire.

Extracting these physical parameters by experiments allows to approach a relatively accurate estimation of self-Joule-heating. Good agreements between numerical simulations (Figure 1, Figure S6) and NO_2 response experiments (Figure2, Figure S6) have been achieved. The successful implementation of numerical simulation on experiments stimulates us to establish the correlation between dimension of device and equilibrium temperature under certain Joule power. By fixing the resistivity of nanowires, assuming the same κ_{SnO2}, center temperature as a function of nanowire length and diameter under constant Joule power of 1 μW (Figure S7((a)) and 10 μW (Figure S7((b)) is calculated. Below Joule power of 1 μW, the temperature of self-heated nanowires (diameter of 40-80 nm and length of < 6000 nm) is lower than 323 K. Increasing the Joule power up to ~10 μW enables an apparent self-Joule-heating up to 400-530 K. We have added the dimension and power consumption of tested self-Joule-heating devices in Figure S7((b). Thinner nanowires clearly show good performance in terms of low power

or energy consumption. Figure S7 could provide a useful guideline for managing thermal properties of nanodevices in future.

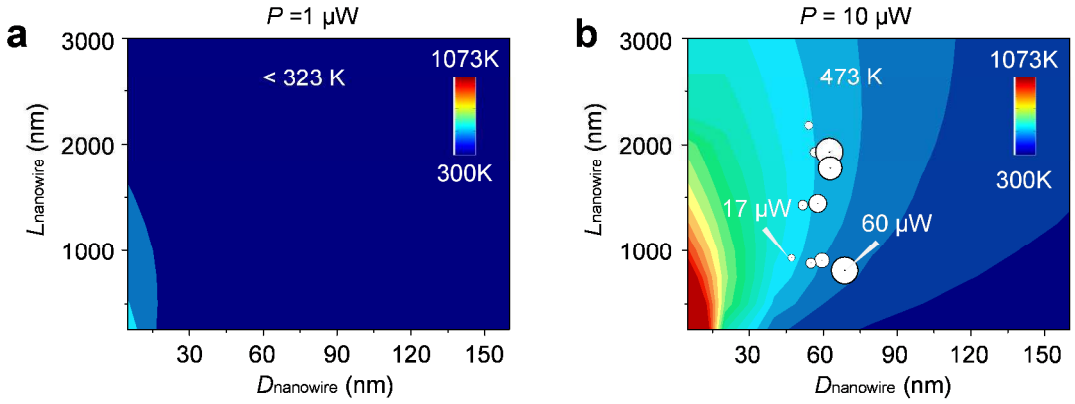

Figure S7. Numerical simulation of center temperature as a function of nanowire diameter and length, under a fixed Joule power of (a) 1 μW and (b) 10 μW. The diameter, length of tested suspended devices and the power consumption are marked by open circles in Figure (b). Size of circle is proportional with power consumption.

Time dependent self-Joule-heating is studied based on the following equation:

$$\rho C_P \frac{\partial T}{\partial t} + \nabla \cdot (-k \nabla T) = Q \qquad \text{(Eq-S6)}$$

where, ρ represents density, C_P is heat capacity, Q is heat sink. Dimension, resistivity of SnO_2 nanowire and applied voltage bias are utilized based on Figure 3. Time scale of thermal relaxation is found to be around ~ μs range, as seen in Figure 2c.

Part III Continuous operation of self-heated SnO_2 nanowire sensor

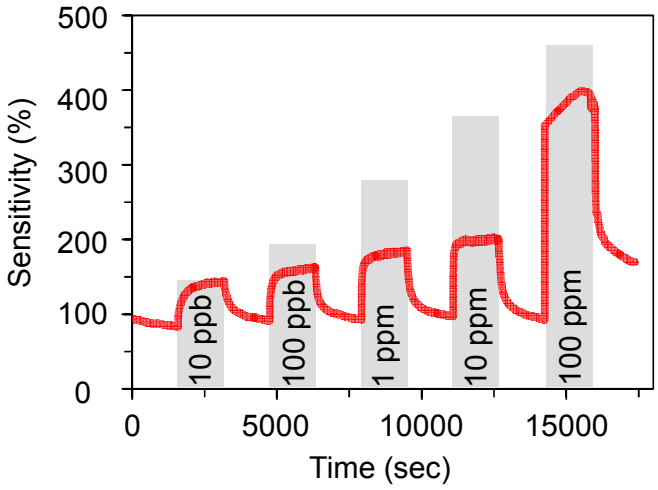

Figure S8. Response of self-heated SnO_2 nanowires to NO_2 with increasing concentrations from 10 ppb to 100 ppm. Gradual increase of the sensitivity upon high NO_2 concentrations and steady recovery of device can be found, indicating a good stability.

Supplementary References

(1) Meng, G.; Yanagida, T.; Nagashima, K.; Yoshida, H.; Kanai, M.; Klamchuen, A.; Zhuge, F. W.; He, Y.; Rahong, S.; Fang, X. D.; Takeda, S.; Kawai, T. Impact of Preferential Indium Nucleation on Electrical Conductivity of Vapor-Liquid-Solid Grown Indium-Tin Oxide Nanowires. *J. Am. Chem. Soc.* **2013**, *135*, 7033-7038.

(2) Klamchuen, A.; Yanagida, T.; Kanai, M.; Nagashima, K.; Oka, K.; Kawai, T.; Suzuki, M.; Hidaka, Y.; Kai, S. Role of surrounding oxygen on oxide nanowire growth. *Appl. Phys. Lett.* **2010**, *97*, 073114.

(3) Prades, J. D.; Jimenez-Diaz, R.; Hernandez-Ramirez, F.; Barth, S.; Cirera, A.; Romano-Rodriguez, A.; Mathur, S.; Morante, J. R. Ultralow power consumption gas sensors based on self-heated individual nanowires. *Appl. Phys. Lett.* **2008**, *93*, 123110.

(4) Suehle, J. S.; Cavicchi, R. E.; Gaitan, M.; Semancik, S. Tin oxide gas sensor fabricated using CMOS micro-hotplates and in-situ processing. *IEEE Electron Device Lett.* **1993**, *14*, 118-120.

(5) Sheng, L. Y.; Tang, Z. N.; Wu, J.; Chan, P. C. H.; Sin, J. K. O. A low-power CMOS compatible integrated gas sensor using maskless tin oxide sputtering. *Sensor Actuat. B-Chem.* **1998**, *49*, 81-87.

(6) Afridi, M. Y.; Suehle, J. S.; Zaghloul, M. E.; Berning, D. W.; Hefner, A. R.; Cavicchi, R. E.; Semancik, S.; Montgomery, C. B.; Taylor, C. J. A Monolithic CMOS Microhotplate-Based Gas Sensor System. *IEEE Sens. J.* **2002**, *2*, 644-655.

(7) Graf, M.; Barrettino, D.; Kirstein, K. U.; Hierlemann, A. CMOS microhotplate sensor system for operating temperatures up to 500 degrees C. *Sensor Actuat. B-Chem.* **2006**, *117*, 346-352.

(8) Mecklenburg, M.; Hubbard, W. A.; White, E. R.; Dhall, R.; Cronin, S. B.; Aloni, S.; Regan, B. C. Nanoscale temperature mapping in operating microelectronic devices. *Science* **2015**, *347*, 629-632.

(9) Haynes, W. M. *CRC Handbook of Chemistry and Physics, 93rd Edition*; Taylor & Francis, 2012.

(10) Surhone, L. M.; Timpledon, M. T.; Marseken, S. F. *Stefan-Boltzmann Law: Stefan-Boltzmann Law, Black Body, Irradiance, Thermodynamic Temperature, Ultraviolet*

Catastrophe, History of Quantum Mechanics, Thermodynamics; Betascript Publishing, 2010.

(11) Rybicki, G. B.; Lightman, A. P. *Radiative processes in astrophysics*; Wiley: New York, 1979.

(12) Turkes, P.; Pluntke, C.; Helbig, R. Thermal-Conductivity of Sno_2 Single-Crystals. *J. Phys. C Solid State* **1980**, *13*, 4941-4951.

(13) Pop, E. Energy dissipation and transport in nanoscale devices. *Nano Research* **2010**, *3*, 147-169.

(14) Lu, L.; Yi, W.; Zhang, D. L. 3 omega method for specific heat and thermal conductivity measurements. *Rev. Sci. Instrum.* **2001**, *72*, 2996-3003.

(15) Li, D. Y.; Wu, Y. Y.; Kim, P.; Shi, L.; Yang, P. D. Thermal conductivity of individual silicon nanowires. *Appl. Phys. Lett.* **2003,** *83*, 2934-2936.